AIAA JOURNAL
Vol. 47, No. 11, November 2009

Numerical Investigation of Decomposed Magnetofluid Dynamics Equations

Ovais U. Khan* and Klaus A. Hoffmann†
Wichita State University, Wichita, Kansas 67260

DOI: 10.2514/1.42626

In addition to the two commonly used formulations for magnetofluid dynamics, a third formulation based on the decomposition of the magnetic field for solving full magnetofluid dynamics equations is explored. The governing equations are transformed to a generalized computational domain and discretized using a finite difference technique. A time-explicit multistage Runge–Kutta scheme augmented with total variation diminishing limiters for time integration is implemented. The developed codes have been validated with the existing closed-form solution of the magnetic Rayleigh problem. Results obtained from the decomposed magnetofluid dynamics equations compare well with results obtained by solving the classical full magnetofluid dynamics equations for a wide range of magnetic Reynolds numbers. It is shown that the decomposed magnetofluid dynamics technique requires substantially less computation time compared with classical full magnetofluid dynamics equations for the solution involving flowfields with high imposed magnetic fields.

Nomenclature

$\mathbf{B}$	=	magnetic field vector, $\begin{Bmatrix} B_x \\ B_y \\ B_z \end{Bmatrix}$
$\mathbf{E}$	=	electric field vector, $\begin{Bmatrix} E_x \\ E_y \\ E_z \end{Bmatrix}$
$\mathbf{E}$	=	convective flux vector in the x direction
$\mathbf{E}_v$	=	diffusion flux vector in the x direction
e_t	=	total energy per unit mass
$\mathbf{F}$	=	convective flux-vector in the y direction
$\mathbf{F}_v$	=	diffusion flux-vector in the y direction
$\mathbf{G}$	=	convective flux vector in the z direction
$\mathbf{G}_v$	=	diffusion flux vector in the z direction
$\bar{\mathbf{I}}$	=	identity tensor
J	=	Jacobian of transformation
$\mathbf{J}$	=	current density vector
M	=	Mach number
Pr	=	Prandtl number
p	=	pressure
$\mathbf{Q}$	=	field vector
Q	=	magnetic interaction parameter, $\frac{\sigma_e B^2 L}{\rho U}$
q	=	dynamic pressure
Re	=	Reynolds number
R_m	=	magnetic Reynolds number
t	=	time
$\mathbf{U}$	=	velocity vector, $\begin{Bmatrix} u \\ v \\ w \end{Bmatrix}$
x, y, z	=	Cartesian coordinates
$\boldsymbol{\nabla}$	=	nabla operator
γ	=	ratio of specific heats
η, ξ, ζ	=	generalized coordinate
η_x, η_y, η_z	=	transformation metrics
μ_{eo}	=	free space magnetic permeability
ξ_x, ξ_y, ξ_z	=	transformation metrics
ρ	=	density
σ_e	=	electrical conductivity

Subscripts

e	=	electromagnetic quantity
i	=	induced magnetic field
o	=	imposed magnetic field
t	=	total magnetic field
v	=	diffusion quantity
∞	=	freestream condition

Superscript

n	=	iteration (time) level

Indices

i	=	index in the ξ direction
j	=	index in the η direction
k	=	index in the ζ direction

Presented as Paper 1068 at the 46th AIAA Aerospace Sciences Meeting and Exhibit, Reno, NV, 7–10 January 2008; received 7 December 2008; revision received 18 March 2009; accepted for publication 31 March 2009.

*Graduate Research Assistant, Department of Aerospace Engineering. Student Member AIAA.

†Marvin J. Gordon Distinguished Professor of Aerospace Engineering, Department of Aerospace Engineering. Associate Fellow AIAA.

I. Introduction

SEVERAL numerical investigations have been dedicated to understanding the magnetofluid dynamics (MFD) of high-speed flows using classical full MFD (FMFD) and low magnetic Reynolds number approaches with different types of magnetic field distributions. Gaitonde and Poggie [1] used FMFD equations of finitely conducting fluid to simulate inviscid flow over a two-dimensional cylindrical body with nonuniform magnetic field distribution. An increase in shock standoff distance, a decrease in surface heat transfer, and a decrease in surface static pressure near the stagnation region were observed with the application of a magnetic field. The low magnetic Reynolds number approach was used by Poggie and Gaitonde [2] to model viscous and inviscid flows over a hemisphere. They illustrated that the application of a magnetic field caused an increase in shock standoff distance for both viscous and inviscid flows and concluded that qualitative changes in the pressure field obtained by applying a magnetic field were negligibly affected by viscous effects for simple blunt-body configurations.

The full MFD equations without Joule heating for two-dimensional blunt-body configurations was investigated by Hoffmann et al. [3]. Different types of magnetic field distributions were used; however, the maximum stand off distance for shock was observed for uniform

magnetic field distribution. They described the low level of electrical conductivity of air as a major source of numerical difficulties in achieving the solution of full MFD equations.

Since the late 1990s, MacCormack has significantly contributed to the theoretical literature of MFD problems by performing various numerical investigations [4–9]. In [4], full MFD equations were used for modeling a viscous MFD flow over the surface of a spherical cone with a dipole type of magnetic field placed at the center of the sphere. An alternate form of full MFD equations to remove the difficulties associated with the application of a strong magnetic field was proposed by MacCormack [5]. It has been pointed out that a significantly low level of electrical conductivity observed in aerodynamic flows requires the application of strong magnetic fields for generating a Lorentz force of considerable strength. However, severe numerical difficulties have been encountered in solving the classical full MFD equations under these circumstances, primarily because of the large order of magnitude of magnetic pressure. Therefore, an alternate form of full MFD equations, described as reduced MFD equations, based on splitting the total magnetic field into imposed and induced components, was introduced; subsequently, the reduced governing equations were solved numerically. Good agreement between classical full MFD equations and an alternate formulation was demonstrated for thrust and axial velocity distributions within an MFD accelerator. Subsequently, the alternate form of full MFD equations was successfully used in several numerical investigations, for example, in [6–9].

It has been widely accepted among numerical investigators of magnetoaerodynamics that the solution of classical full MFD equations with strong imposed magnetic fields is not a simple task for weakly ionized flows, which occur in most aerodynamic applications [3,5–7,10]. The large magnitude of magnetic pressure occurs as a result of the proportionality of the magnetic pressure to the square of the applied magnetic field, or mathematically as

$$p_{\text{mag}} = (1/2\mu_{eo})B^2$$

With the application of a strong imposed magnetic field, the magnetic pressure can be several orders of magnitude larger than the aerodynamic pressure or the induced magnetic field pressure. Thus, numerical errors associated with very large magnetic pressure terms could be significant when compared with relatively smaller fluid stress terms, potentially resulting in instability of the numerical scheme. On the other hand, at low values of electrical conductivity, other difficulties in solving the magnetic induction equation occur because of the exceedingly high coefficient of magnetic diffusion. Thus, it is necessary to explore an alternate full MFD system of equations that not only accounts for the presence of the induced magnetic field but also provides an efficient way to avoid numerical degenerations associated with the aforementioned difficulties. In the current effort, the alternate formulation has been termed "decomposed MFD equations."

II. Governing Equations

One of the objectives of the present work is to implement the decomposed MFD (DMFD) equations using an explicit modified Runge–Kutta scheme. First, the formulation of the governing equations is developed, and the transformation to a generalized curvilinear domain is discussed. Subsequently, a numerical algorithm based on a fourth-order modified Runge–Kutta scheme augmented with a TVD limiter in the postprocessing stage has been developed for the DMFD equations. An explicit time-marching numerical scheme is used to achieve the solutions for various flow problems.

A. Decomposed Magnetofluid Dynamics Equations

Decomposition of the total magnetic field has been introduced according to

$$B_t = B_i + B_o$$

where B_i is the induced magnetic field, B_o is the imposed magnetic field, and B_t is the total magnetic field. Following this strategy, the total magnetic field is split into imposed and induced magnetic field components in all respective directions. For applications in which the induced magnetic field is not negligible, the Lorentz force can be rewritten as

$$\mathbf{F}_{\text{Lorentz}} = (1/\mu_e)(\boldsymbol{\nabla} \times \mathbf{B}_t) \times \mathbf{B}_t$$

Subsequent to introducing the magnetic field splitting, this can be written as

$$\mathbf{F}_{\text{Lorentz}} = (1/\mu_e)(\boldsymbol{\nabla} \times \mathbf{B}_i) \times \mathbf{B}_t$$

Because the imposed magnetic field is generated by currents outside the flowfield, $\boldsymbol{\nabla} \times \mathbf{B}_o = 0$. By substituting this expression for the Lorentz force into the momentum and energy equations and using the divergence and curl free nature of the imposed magnetic field (adjusting the magnetic terms equivalent to fluid dynamics terms), the decomposed MFD equations can be rearranged as follows.

Continuity equation:

$$\frac{\partial \rho}{\partial t} + \boldsymbol{\nabla} \cdot (\rho \mathbf{U}) = 0 \tag{1}$$

Momentum equation:

$$\frac{\partial(\rho \mathbf{U})}{\partial t} + \boldsymbol{\nabla} \cdot (\rho \mathbf{U} \otimes \mathbf{U} + (p + p_{\text{mag}})\bar{\bar{\mathbf{I}}}) - \frac{\mathbf{B}_i \otimes \mathbf{B}_t}{\mu_{eo}} - \frac{\mathbf{B}_o \otimes \mathbf{B}_i}{\mu_{eo}} = \boldsymbol{\nabla} \cdot \bar{\bar{\boldsymbol{\tau}}} \tag{2}$$

Induction equation:

$$\frac{\partial \mathbf{B}_i}{\partial t} + \boldsymbol{\nabla} \cdot (\mathbf{U} \otimes \mathbf{B}_t - \mathbf{B}_t \otimes \mathbf{U}) = \nu_e \nabla^2 \mathbf{B}_i \tag{3}$$

Energy equation:

$$\frac{\partial}{\partial t}(\rho e_t) + \boldsymbol{\nabla} \cdot \left[(\rho e_t + p + p_{\text{mag}})\mathbf{U} + \frac{\mathbf{B}_t}{\mu_{eo}}(\mathbf{U} \cdot \mathbf{B}_i) \right] = \boldsymbol{\nabla} \cdot (\bar{\bar{\boldsymbol{\tau}}} \cdot \mathbf{U}) + \boldsymbol{\nabla} \cdot \mathbf{q} + \frac{\nu_e}{\mu_{eo}}(\boldsymbol{\nabla} \times \mathbf{B}_i)^2 \tag{4}$$

where

$$p_{\text{mag}} = -(1/2\mu_{eo})B_i^2 + (1/\mu_{eo})\mathbf{B}_i \cdot \mathbf{B}_t \tag{5}$$

and

$$\rho e_t = \frac{1}{2}\rho U^2 + \frac{p}{\gamma - 1} + \frac{B_i^2}{2\mu_{eo}} \tag{6}$$

It is interesting to note that, subsequent to replacing the total magnetic pressure $(1/2\mu_{eo})B_t^2$ with the smaller quantity $-(1/2\mu_{eo})B_i^2 + (1/\mu_{eo})\mathbf{B}_i \cdot \mathbf{B}_t$, the magnetic and aerodynamic pressures become similar in magnitude for strong imposed magnetic fields. Furthermore, magnetic stress terms become a function of induced magnetic fields, only because $\nu_e(\boldsymbol{\nabla} \times \mathbf{B}_t) = \nu_e(\boldsymbol{\nabla} \times \mathbf{B}_i)$, which will eventually produce beneficial effects on stability because not only are the production and diffusion terms of magnetic induction equation similar, but Joulean dissipation becomes a function of the induced magnetic field only.

Subsequently, the DMFD equations are nondimensionalized according to the procedure outlined in [11]. In the subsequent sections, all equations will be in the nondimensional form unless otherwise specified. The nondimensional DMFD equations can be represented in a compact vector form in three-dimensional Cartesian coordinates as

$$\frac{\partial \mathbf{Q}}{\partial t} + \frac{\partial \mathbf{E}}{\partial x} + \frac{\partial \mathbf{F}}{\partial y} + \frac{\partial \mathbf{G}}{\partial z} = \frac{\partial \mathbf{E}_v}{\partial x} + \frac{\partial \mathbf{F}_v}{\partial y} + \frac{\partial \mathbf{G}_v}{\partial z} \tag{7}$$

where $\mathbf{Q}$ is the unknown flux vector

$$\mathbf{Q} = [\rho \quad \rho u \quad \rho v \quad \rho w \quad B_{ix} \quad B_{iy} \quad B_{iz} \quad \rho e_t]^T \tag{8a}$$

and

$$\rho e_t = \tfrac{1}{2}\rho U^2 + (p/(\gamma-1)) + (B_i^2/2) \tag{8b}$$

$\mathbf{E}$, $\mathbf{F}$, and $\mathbf{G}$ are the inviscid flux vectors, and $\mathbf{E}_v$, $\mathbf{F}_v$, and $\mathbf{G}_v$ are the diffusion flux vectors. The following are the details for the flux vectors:

$$\mathbf{E} = \begin{Bmatrix} \rho u \\ \rho u^2 + p^* - B_{ix}B_{tx} - B_{ix}B_{ox} \\ \rho uv - B_{iy}B_{tx} - B_{ix}B_{oy} \\ \rho uw - B_{iz}B_{tx} - B_{ix}B_{oz} \\ 0 \\ uB_{ty} - vB_{tx} \\ uB_{tz} - wB_{tx} \\ (\rho e_t + p^*)u - B_{tx}(uB_{ix} + vB_{iy} + wB_{iz}) \end{Bmatrix} \tag{8c}$$

$$\mathbf{F} = \begin{Bmatrix} \rho v \\ \rho vu - B_{ix}B_{ty} - B_{iy}B_{ox} \\ \rho v^2 + p^* - B_{iy}B_{ty} - B_{iy}B_{oy} \\ \rho vw - B_{iz}B_{ty} - B_{iy}B_{oz} \\ vB_{tx} - uB_{ty} \\ 0 \\ vB_{tz} - wB_{ty} \\ (\rho e_t + p^*)v - B_{ty}(uB_{ix} + vB_{iy} + wB_{iz}) \end{Bmatrix} \tag{8d}$$

$$\mathbf{G} = \begin{Bmatrix} \rho w \\ \rho uw - B_{ix}B_{tz} - B_{iz}B_{ox} \\ \rho vw - B_{iy}B_{tz} - B_{iz}B_{oy} \\ \rho w^2 + p^* - B_{iz}B_{tz} - B_{iz}B_{oz} \\ wB_{tx} - uB_{tz} \\ wB_{ty} - vB_{tz} \\ 0 \\ (\rho e_t + p^*)w - B_{tz}(uB_{ix} + vB_{iy} + wB_{iz}) \end{Bmatrix} \tag{8e}$$

$$\mathbf{E}_v = \begin{Bmatrix} 0 \\ \tau_{xx} \\ \tau_{xy} \\ \tau_{xz} \\ 0 \\ \frac{1}{R_m\sigma_e}\left(\frac{\partial B_{iy}}{\partial x} - \frac{\partial B_{ix}}{\partial y}\right) \\ \frac{1}{R_m\sigma_e}\left(\frac{\partial B_{iz}}{\partial x} - \frac{\partial B_{ix}}{\partial z}\right) \\ u\tau_{xx} + v\tau_{xy} + w\tau_{xz} + q_x + q_{Jx} \end{Bmatrix} \tag{8f}$$

$$\mathbf{F}_v = \begin{Bmatrix} 0 \\ \tau_{yx} \\ \tau_{yy} \\ \tau_{yz} \\ \frac{1}{R_m\sigma_e}\left(\frac{\partial B_{ix}}{\partial y} - \frac{\partial B_{iy}}{\partial x}\right) \\ 0 \\ \frac{1}{R_m\sigma_e}\left(\frac{\partial B_{iz}}{\partial y} - \frac{\partial B_{iy}}{\partial z}\right) \\ u\tau_{yx} + v\tau_{yy} + w\tau_{yz} + q_y + q_{Jy} \end{Bmatrix} \tag{8g}$$

$$\mathbf{G}_v = \begin{Bmatrix} 0 \\ \tau_{zx} \\ \tau_{zy} \\ \tau_{zz} \\ \frac{1}{R_m\sigma_e}\left(\frac{\partial B_{ix}}{\partial z} - \frac{\partial B_{iz}}{\partial x}\right) \\ \frac{1}{R_m\sigma_e}\left(\frac{\partial B_{iy}}{\partial z} - \frac{\partial B_{iz}}{\partial y}\right) \\ 0 \\ u\tau_{zx} + v\tau_{zy} + w\tau_{zz} + q_z + q_{Jz} \end{Bmatrix} \tag{8h}$$

where

$$p^* = p - \tfrac{1}{2}B_i^2 + \mathbf{B}_i \cdot \mathbf{B}_t \tag{9a}$$

For a Newtonian fluid with Stokes hypothesis, the viscous stress tensor can be written as

$$\tau_{ij} = \frac{1}{Re_\infty}\left(\mu\left(\frac{\partial u_i}{\partial x_j} + \frac{\partial u_j}{\partial x_i}\right) - \delta_{ij}\frac{2}{3}\mu\frac{\partial u_k}{\partial x_k}\right) \tag{9b}$$

For a perfect gas, the heat transfer rate can be written as

$$q_i = \frac{\mu}{Re_\infty Pr(\gamma-1)M_\infty^2}\frac{\partial T}{\partial x_i} \tag{9c}$$

Joule heating becomes a function of the induced magnetic field and may be expressed as

$$q_{J_i} = \frac{B_{i_j}}{R_m\sigma_e}\left(\frac{\partial B_{i_j}}{\partial x_i} - \frac{\partial B_{i_i}}{\partial x_j}\right) \tag{9d}$$

Subscripts i, j, and k are used for convenience to define terms using Einstein summation convention. It is important to note that the imposed magnetic field cannot be eliminated entirely from the governing equations due to the nonlinear behavior of the magnetic field; however, no products of the imposed magnetic field will appear in the governing equations.

1. Modification to Decomposed Magnetofluid Dynamics Equations with $\nabla \cdot \mathbf{B}$ Condition

Similar to the full MFD equations, the aforementioned DMFD system has eight scalar equations with a seven-wave structure, because Jacobian matrices have a singularity associated with the normal component of a magnetic field. Therefore, a modification in DMFD equations is required to remove the singularity. In the present work, the technique by Powell et al. [12] of introducing Gauss's law of magnetism to modify the Jacobian matrices has been used and implemented for the DMFD equations. This amendment results in an additional term in the flux vector form of the DMFD equations that ultimately results in nonsingular Jacobian matrices. Mathematically, it follows as

$$\frac{\partial}{\partial t}\begin{bmatrix} \rho \\ \rho\mathbf{U} \\ \mathbf{B}_i \\ \rho e_t \end{bmatrix} + \nabla \cdot \begin{bmatrix} \rho\mathbf{U} \\ \rho\mathbf{U}\otimes\mathbf{U} + (p + p_{\text{mag}})\bar{\bar{\mathbf{I}}} - \frac{1}{\mu_{e0}}\mathbf{B}_i \otimes \mathbf{B}_t - \frac{1}{\mu_{e0}}\mathbf{B}_o \otimes \mathbf{B}_i \\ \mathbf{U}\otimes\mathbf{B}_t - \mathbf{B}_t \otimes \mathbf{U} \\ (\rho e_t + p + p_{\text{mag}})\mathbf{U} - \frac{\mathbf{B}_t}{\mu_{e0}}(\mathbf{U}\cdot\mathbf{B}_i) \end{bmatrix} + \begin{bmatrix} 0 \\ \mathbf{B}_t \\ \mathbf{U} \\ \mathbf{U}\cdot\mathbf{B}_t \end{bmatrix}\nabla\cdot\mathbf{B}_i = \begin{bmatrix} 0 \\ \nabla\cdot\bar{\bar{\boldsymbol{\tau}}} \\ \nu_e\nabla^2\mathbf{B}_i \\ \nabla\cdot(\mathbf{U}\cdot\bar{\bar{\boldsymbol{\tau}}}) - \nabla\cdot\mathbf{q} + \frac{\nu_e}{\mu_{eo}}(\nabla\times\mathbf{B}_i)^2 \end{bmatrix} \tag{10}$$

With inclusion of the term $\mathbf{H}$ for removing the singularity, Eq. (7) can be written as

$$\frac{\partial \mathbf{Q}}{\partial t}+\frac{\partial \mathbf{E}}{\partial x}+\frac{\partial \mathbf{F}}{\partial y}+\frac{\partial \mathbf{G}}{\partial z}+\mathbf{H}=\frac{\partial \mathbf{E}_v}{\partial x}+\frac{\partial \mathbf{F}_v}{\partial y}+\frac{\partial \mathbf{G}_v}{\partial z} \tag{11}$$

where

$$\mathbf{H}=\mathbf{H}_M\left(\frac{\partial B_{ix}}{\partial x}+\frac{\partial B_{iy}}{\partial y}+\frac{\partial B_{iz}}{\partial z}\right) \tag{12a}$$

and

$$\mathbf{H}_M=\begin{Bmatrix}0\\ B_{tx}\\ B_{ty}\\ B_{tz}\\ u\\ v\\ w\\ (uB_{tx}+vB_{ty}+wB_{tz})\end{Bmatrix} \tag{12b}$$

Observe that the additional term $\mathbf{H}$ also becomes a function of the induced magnetic field due to the divergence-free nature of the imposed magnetic field; that is, $\nabla\cdot\mathbf{B}_o=0$.

B. Curvilinear Coordinates

The nondimensional DMFD equations have been transformed from physical space (x, y, z) to generalized computational space (ξ, η, ζ). The transformed equations are

$$\frac{\partial \bar{\mathbf{Q}}}{\partial t}+\frac{\partial \bar{\mathbf{E}}}{\partial \xi}+\frac{\partial \bar{\mathbf{F}}}{\partial \eta}+\frac{\partial \bar{\mathbf{G}}}{\partial \zeta}+\bar{\mathbf{H}}=\frac{\partial \bar{\mathbf{E}}_v}{\partial \xi}+\frac{\partial \bar{\mathbf{F}}_v}{\partial \eta}+\frac{\partial \bar{\mathbf{G}}_v}{\partial \zeta} \tag{13}$$

where

$$\bar{\mathbf{Q}}=(\mathbf{Q}/J) \tag{14a}$$

$$\bar{\mathbf{E}}=\tfrac{1}{J}(\xi_x\mathbf{E}+\xi_y\mathbf{F}+\xi_z\mathbf{G}) \tag{14b}$$

$$\bar{\mathbf{F}}=\tfrac{1}{J}(\eta_x\mathbf{E}+\eta_y\mathbf{F}+\eta_z\mathbf{G}) \tag{14c}$$

$$\bar{\mathbf{G}}=\tfrac{1}{J}(\zeta_x\mathbf{E}+\zeta_y\mathbf{F}+\zeta_z\mathbf{G}) \tag{14d}$$

$$\bar{\mathbf{H}}=\bar{\mathbf{H}}_M\left(\frac{\partial \bar{B}_{ix}}{\partial \xi}+\frac{\partial \bar{B}_{iy}}{\partial \eta}+\frac{\partial \bar{B}_{iz}}{\partial \zeta}\right) \tag{14e}$$

$$\bar{B}_{ix}=\tfrac{1}{J}(\xi_xB_{ix}+\xi_yB_{iy}+\xi_zB_{iz}) \tag{14f}$$

$$\bar{B}_{iy}=\tfrac{1}{J}(\eta_xB_{ix}+\eta_yB_{iy}+\eta_zB_{iz}) \tag{14g}$$

$$\bar{B}_{iz}=\tfrac{1}{J}(\zeta_xB_{ix}+\zeta_yB_{iy}+\zeta_zB_{iz}) \tag{14h}$$

$$\bar{\mathbf{E}}_v=\tfrac{1}{J}(\xi_x\mathbf{E}_v+\xi_y\mathbf{F}_v+\xi_z\mathbf{G}_v) \tag{14i}$$

$$\bar{\mathbf{F}}_v=\tfrac{1}{J}(\eta_x\mathbf{E}_v+\eta_y\mathbf{F}_v+\eta_z\mathbf{G}_v) \tag{14j}$$

$$\bar{\mathbf{G}}_v=\tfrac{1}{J}(\zeta_x\mathbf{E}_v+\zeta_y\mathbf{F}_v+\zeta_z\mathbf{G}_v) \tag{14k}$$

$\bar{\mathbf{E}}$, $\bar{\mathbf{F}}$, and $\bar{\mathbf{G}}$ represent the convective flux vectors, and $\bar{\mathbf{E}}_v$, $\bar{\mathbf{F}}_v$, and $\bar{\mathbf{G}}_v$ are the diffusion flux vectors. Each flux vector has eight components. Evaluation of the convective flux terms is obtained from Eqs. (14b–14d). However, the diffusion flux terms involve spatial derivatives of the velocity and magnetic field; therefore, these derivatives must be transformed into the computational domain, the procedure of which has been outlined in [13]. The expressions of the diffusion flux vectors in generalized space are provided in [11].

Finally, the DMFD Eq. (13) can be rewritten by definition of the flux Jacobian matrices as

$$\frac{\partial \bar{\mathbf{Q}}}{\partial t}+\bar{\mathbf{A}}\frac{\partial \bar{\mathbf{Q}}}{\partial \xi}+\bar{\mathbf{B}}\frac{\partial \bar{\mathbf{Q}}}{\partial \eta}+\bar{\mathbf{C}}\frac{\partial \bar{\mathbf{Q}}}{\partial \zeta}=\frac{\partial \bar{\mathbf{E}}_v}{\partial \xi}+\frac{\partial \bar{\mathbf{F}}_v}{\partial \eta}+\frac{\partial \bar{\mathbf{G}}_v}{\partial \zeta} \tag{15}$$

where

$$\bar{\mathbf{A}}=\frac{\partial \bar{\mathbf{E}}}{\partial \bar{\mathbf{Q}}}+\mathbf{H}_M\frac{\partial \bar{B}_{ix}}{\partial \bar{\mathbf{Q}}}=\xi_x\mathbf{A}+\xi_y\mathbf{B}+\xi_z\mathbf{C} \tag{16a}$$

$$\bar{\mathbf{B}}=\frac{\partial \bar{\mathbf{F}}}{\partial \bar{\mathbf{Q}}}+\mathbf{H}_M\frac{\partial \bar{B}_{iy}}{\partial \bar{\mathbf{Q}}}=\eta_x\mathbf{A}+\eta_y\mathbf{B}+\eta_z\mathbf{C} \tag{16b}$$

$$\bar{\mathbf{C}}=\frac{\partial \bar{\mathbf{G}}}{\partial \bar{\mathbf{Q}}}+\mathbf{H}_M\frac{\partial \bar{B}_{iz}}{\partial \bar{\mathbf{Q}}}=\zeta_x\mathbf{A}+\zeta_y\mathbf{B}+\zeta_z\mathbf{C} \tag{16c}$$

$$\mathbf{A}=\frac{\partial \mathbf{E}}{\partial \mathbf{Q}}+\mathbf{H}_M\frac{\partial B_{ix}}{\partial \mathbf{Q}} \tag{16d}$$

$$\mathbf{B}=\frac{\partial \mathbf{F}}{\partial \mathbf{Q}}+\mathbf{H}_M\frac{\partial B_{iy}}{\partial \mathbf{Q}} \tag{16e}$$

$$\mathbf{C}=\frac{\partial \mathbf{G}}{\partial \mathbf{Q}}+\mathbf{H}_M\frac{\partial B_{iz}}{\partial \mathbf{Q}} \tag{16f}$$

$\bar{\mathbf{A}}$, $\bar{\mathbf{B}}$, and $\bar{\mathbf{C}}$ are the flux Jacobian matrices in the generalized curvilinear domain, whereas $\mathbf{A}$, $\mathbf{B}$, and $\mathbf{C}$ are the flux Jacobian matrices in the physical domain. Note that only induced magnetic field components need to be transformed because partial derivatives of imposed magnetic field components have disappeared in the physical domain.

III. Numerical Method

The modified Runge–Kutta scheme stabilized with a total variation diminishing (TVD) scheme for damping the numerical oscillations associated with convective fluxes has been developed to obtain numerical solutions of DMFD equations. The TVD model is based on the eigenvalues and eigenvectors of the flux Jacobian matrices associated with the convective part of the DMFD equations. The details of linearization and procedure for the evaluation of eigenvalues and eigenvectors are provided in [11]. The scheme can be expressed as

$$\bar{\mathbf{Q}}^{(0)}_{i,j,k}=\bar{\mathbf{Q}}^{n}_{i,j,k} \tag{17a}$$

for $m=1$–4 and $\alpha_m=4$–1.

$$\bar{\mathbf{Q}}^{(m)}_{i,j,k}=\bar{\mathbf{Q}}^{n}_{i,j,k}-(\Delta t/\alpha_m)\bar{f}^{(m-1)}_{i,j,k} \tag{17b}$$

where

$$\bar{f} = \frac{\partial \bar{\mathbf{E}}}{\partial \xi} + \frac{\partial \bar{\mathbf{F}}}{\partial \eta} + \frac{\partial \bar{\mathbf{G}}}{\partial \zeta} + \bar{\mathbf{H}} - \frac{\partial \bar{\mathbf{E}}_v}{\partial \xi} - \frac{\partial \bar{\mathbf{F}}_v}{\partial \eta} - \frac{\partial \bar{\mathbf{G}}_v}{\partial \zeta} \tag{17c}$$

Second-order central difference approximations have been used for the convective and diffusion terms according to the procedure outlined in [13].

The postprocessing stage is the last stage of computation. Mathematically, it can be expressed as

$$\bar{\mathbf{Q}}_{i,j,k}^{n+1} = \bar{\mathbf{Q}}_{i,j,k}^{(4)} + \overline{\mathrm{TVD}}^n \tag{17d}$$

Harada et al. [14] have investigated three different TVD schemes along with several TVD limiters for each scheme. In the current investigation, the Davis-Yee symmetric TVD scheme is implemented.

IV. Applications

The second objective of the present work is the validation of the decomposed MFD formulation and the numerical scheme. The DMFD formulation will be validated with the available closed-form solution of the magnetic Rayleigh problem; subsequently, the solution will be compared with the classical FMFD solution. The third objective of the present effort is an efficiency study that considers the magnetic Rayleigh problem as a benchmark case for determining the computational performance of DMFD, FMFD, and low magnetic Reynolds number formulations for weak and strong imposed magnetic fields.

Finally, a blunt-body configuration subjected to hypersonic flow has been selected as a second case in which further validity of the DMFD equations has been examined in comparison with the FMFD equations.

A. Validation of Magnetofluid Dynamics Algorithms

Because of its simplicity and the availability of the closed-form solution, the magnetic Rayleigh problem has been selected for validating the developed computer algorithm based on the DMFD approach of magnetofluid dynamics. The magnetic Rayleigh problem considers an incompressible and viscous fluid over a flat plate suddenly set in motion with a magnetic field imposed normal to the plate surface. In addition to the applied magnetic field, which remains constant, the velocity field induces a magnetic field that travels normal to the plate surface with a constant speed of $A_o = B_o/\sqrt{\mu_{eo}\rho}$ (known as an Alfvén wave). The load factor is zero, that is, the imposed electric field is set equal to zero. The analytical solution available in the literature assumes equal thicknesses of the magnetic and velocity boundary layers, which results in a magnetic Prandtl number of 1. The details of the velocity and induced magnetic field expressions are provided in [15].

A computational block of $10 \times 150 \times 5$ grid spacing with clustering near the solid wall has been generated for the present study. Computations have been initiated at $t = 0.0$ s and continued to the final time period of 0.1 s. The value of the interaction parameter is found to be equal to $Q_{\mathrm{ref}} = 1043.84$. Figure 1 illustrates the velocity distributions with respect to time for the case of an electrically insulating wall. Excellent agreement between the solutions obtained from decomposed MFD equations and the exact relation is demonstrated for all time levels. For example, at a point at which the domain height (y) is equal to 0.5 m, the percentage error between the numerical solution obtained from the DMFD equations and the exact solution is negligible ($\sim$0.16%) for all time levels.

Similarly, an excellent agreement between the numerical and analytical solutions has been observed for the induced magnetic field in the x direction for all time levels, as shown in Fig. 2. It is interesting to observe that equal thicknesses of velocity and magnetic boundary layers have been computed from the DMFD approach, which confirms the underlying assumption in the exact solution.

Subsequent to validating the developed computer code for the DMFD equations with the analytical model, a case involving a significantly lower magnetic Reynolds number (2.5×10^{-3}) has been chosen for attaining further confidence over the DMFD formulation. The electrical conductivity of the medium has been adjusted to achieve a low value of magnetic Reynolds number, and the corresponding value of magnetic interaction parameter is found to be equal to $Q_{\mathrm{ref}} = 1.044$. Figure 3 represents nondimensional

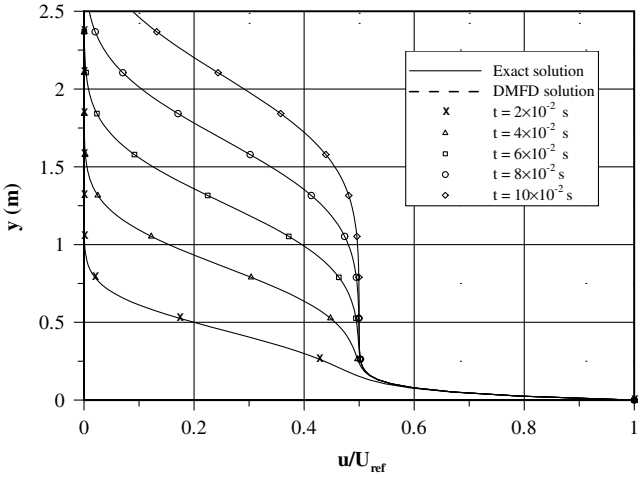

Fig. 1 Comparison of velocity distributions at different time intervals for $R_m = 2.5$.

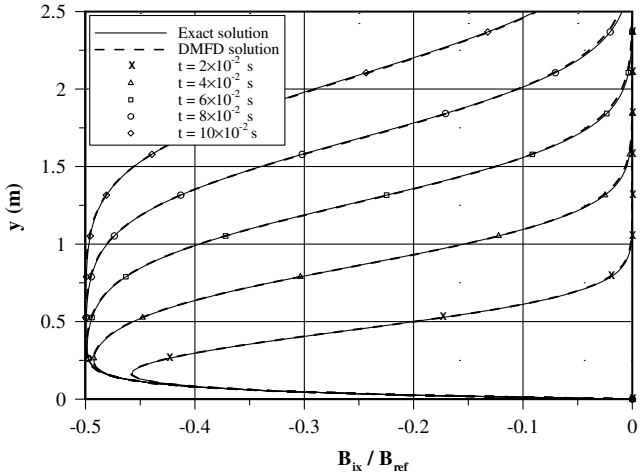

Fig. 2 Comparison of induced magnetic field distributions at different time intervals for $R_m = 2.5$.

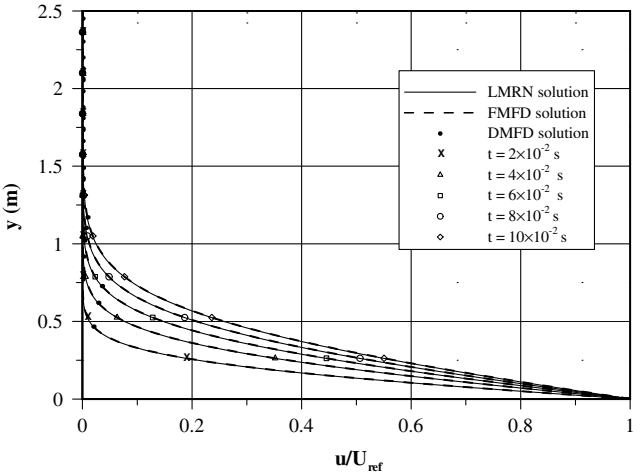

Fig. 3 Comparison of velocities obtained by the DMFD, FMFD, and low magnetic Reynolds number formulations at $R_m = 2.5 \times 10^{-3}$.

velocity profiles obtained from the three available modeling approaches of magnetofluid dynamics for $R_m = 2.5 \times 10^{-3}$. It is obvious that the DMFD formulation also provides similar results compared with the classical full MFD equations and low magnetic Reynolds number approximation for a substantially low range of magnetic Reynolds numbers. Note that all three formulations predict similar results because the induced magnetic field for $R_m = 2.5 \times 10^{-3}$ is substantially smaller than the high values of the induced magnetic field for a magnetic Reynolds number of $R_m = 2.5$.

Furthermore, a nondimensional induced magnetic field along the x direction obtained from the two MFD formulations has been compared in Fig. 4 for different time levels. The induced magnetic field distributions obtained from the DMFD equations compare well with the solution of FMFD equations. Observe that the strength of the induced magnetic field is substantially low for a significantly smaller magnetic Reynolds number ($R_m = 2.5 \times 10^{-3}$). A smaller value of magnetic Reynolds number indicates that the dissipation of the induced magnetic field supersedes the advection.

Finally, a comparison of computational time in terms of wall clock time for achieving the time interval of $t = 0.02$ s from the three modeling approaches is illustrated in Fig. 5. Time has been estimated on a dual core microprocessor of 3.2 GHz speed with 3 GB of RAM, with the optimization option of the compiler used to increase the execution speed.

It is obvious that low magnetic Reynolds number approximation requires substantially less time compared with both full MFD sets of equations for low ranges of magnetic Reynolds numbers. For example, at $R_m = 2.5 \times 10^{-3}$, the computational time taken by both the FMFD and DMFD formulations is ~50.0 h, whereas the computational time required by the low magnetic Reynolds number approach is 0.1 h. As a result, a difference of approximately 50.0 h in computational time is observed, which is very large and may increase further for complex MFD flows. However, with the increase in magnetic Reynolds numbers, the FMFD and DMFD approaches have shown stability, resulting in a relatively larger step size and less amount of wall clock time to reach the desired solution. It is interesting to observe that, as the magnetic Reynolds number approaches 1, all three MFD approaches require a similar amount of time. In fact, the difference in wall clock time for magnetic Reynolds numbers close to 1 is found in the neighborhood of ~0.1 h.

It should be noted that the wall clock time presented in Fig. 5 has been computed for a substantially low strength of the applied magnetic field ($B_o = 1.449 \times 10^{-4}$ T), and it has been found that DMFD equations require a similar amount of time as the FMFD equations for different ranges of magnetic Reynolds numbers for the MFD Rayleigh problem. However, this argument remains valid only for a weak, applied magnetic field; further investigations with a strong, applied magnetic field have shown a substantial reduction in computational time when the DMFD approach is used as compared with the FMFD approach. Because magnetic pressure is directly proportional to the square of magnetic field intensity, when a strong magnetic field is imposed, the magnitude of magnetic pressure may become several orders higher than the static pressure, which may cause instability in the numerical scheme of the FMFD equations. Consequently, a smaller time step is required to overcome this issue, which will ultimately increase the amount of time to achieve the solution from the FMFD formulation. On the other hand, DMFD equations can provide an alternate way of solving the full MFD equations within permissible limits of time with strong imposed magnetic fields.

Figure 6 shows a comparison of wall clock time for three MFD solution approaches for different magnetic Reynolds numbers with a relatively stronger imposed magnetic field intensity ($B_o = 1.3944 \times 10^{-2}$ T). The wall clock time was computed on a dual core microprocessor with a compiler optimization option for attaining a time interval of $t = 0.02$ s. For low ranges of magnetic Reynolds numbers, the DMFD formulation requires less computation time compared with the FMFD formulation. For example, at $R_m = 0.125$, the computation time of the FMFD equations is ~10 times greater than the computation time of the DMFD equations. Note that the difference in computation time of the two full MFD equations significantly increases when values of magnetic Reynolds number are decreased further. It has been observed that the numerical scheme for the FMFD approach shows great instability when a strong magnetic field at low values of magnetic Reynolds numbers is applied, thus making a smaller time step an essential requirement. However, the numerical scheme based on the DMFD equations has shown improvement in stability with a strong imposed magnetic field

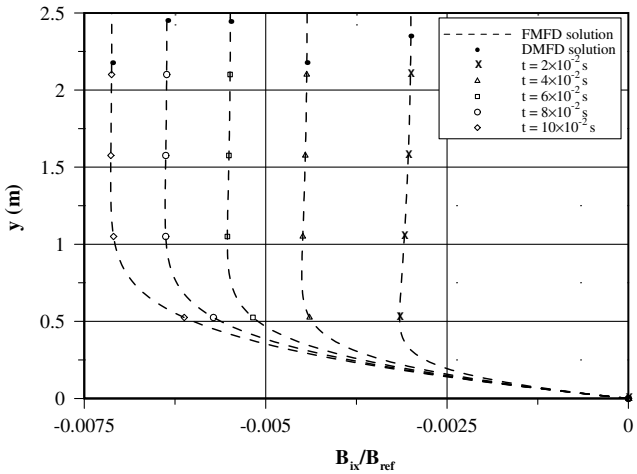

Fig. 4 Comparison of the induced magnetic field distributions obtained by the DMFD and FMFD formulations at $R_m = 2.5 \times 10^{-3}$.

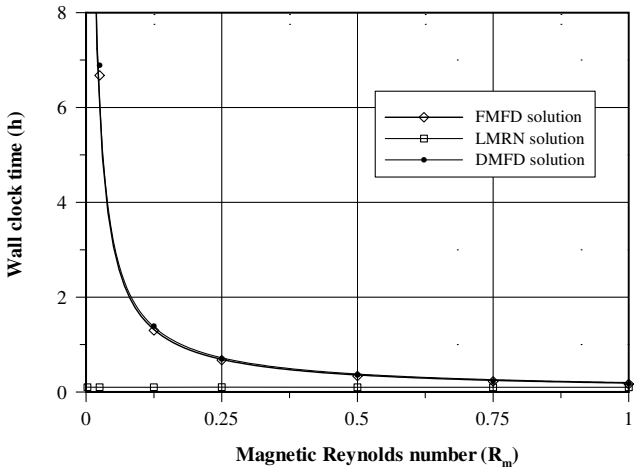

Fig. 5 Wall clock time for the DMFD, FMFD, and low magnetic Reynolds number formulations for $B_o = 1.449 \times 10^{-4}$ T.

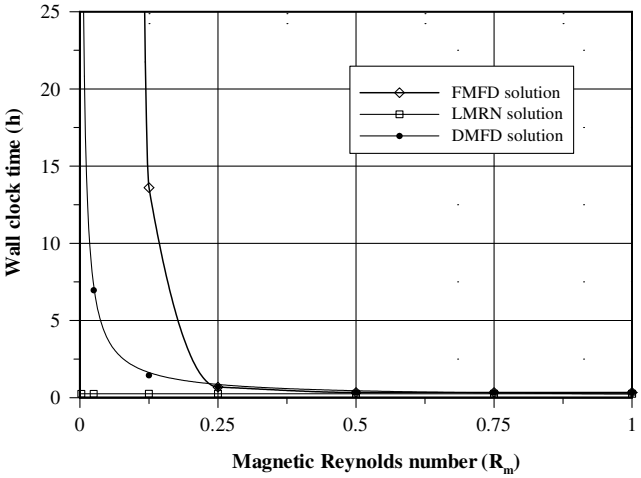

Fig. 6 Wall clock time for the DMFD, FMFD, and low magnetic Reynolds number formulations for $B_o = 1.3944 \times 10^{-2}$ T.

at low values of magnetic Reynolds numbers. Thus, a relatively larger time step can be used to obtain the required solution. Subsequently, the differences in wall clock time for both full MFD approaches start to diminish as magnetic Reynolds numbers begin to increase.

B. Hypersonic Blunt-Body Flow

A blunt-body configuration has been selected as a second case for the current numerical investigation. Hypersonic flow over a two-dimensional blunt body with a uniform magnetic field distribution along the y axis has been considered, and the following operating conditions have been used:

Pressure: $p_\infty = 36.6$ Pa
Electrical conductivity: $\sigma_e = 2800.12$ S/m
Temperature: $T_\infty = 294.0$ K
Reference length: $L_{\text{ref}} = 0.1395$ m
Mach number: $M_\infty = 10.6$
Reynolds number: $Re_{\text{ref}} = 1.213 \times 10^4$

The radius of the body and deflection angle were set equal to 0.1395 m and 15 deg, respectively. A computational grid of 90×70 spacing for blunt-body flow simulations was selected for computations and is depicted in Fig. 7. Clustering near the body surface was enforced to capture viscous effects. Pressure contours for the Navier–Stokes analysis are depicted in Fig. 8. Pressure near the stagnation region has a maximum value, which is consistent with the theory, and has been found to be in good agreement with the available exact relations. The grid was selected after several grid independence studies, the details of which are discussed in the following section.

1. *Navier–Stokes Analysis*

To obtain an economical grid for the computations, a grid independence test was performed before conducting the MFD analysis. Figure 9 represents nondimensional surface pressure along the body surface for the Navier–Stokes analysis; dynamic pressure was used to nondimensionalize the values. It is evident from the figure that an increase in the number of grid points up to 150×110 did not affect the pressure distribution, and a convergence in the pressure values is obvious. Because the results obtained with a mesh size of 90×70 are practically identical with the mesh size of 150×110, a grid of 90×70 was selected for all subsequent analyses.

Furthermore, the numerical result was validated with the exact solution. Figure 9 shows a comparison of the numerical surface pressure with the normal shock data and Newtonian pressure available in the literature. As shown, the numerical pressure calculated for the Navier–Stokes analysis agrees very well with the Newtonian theory and normal shock data near the stagnation region.

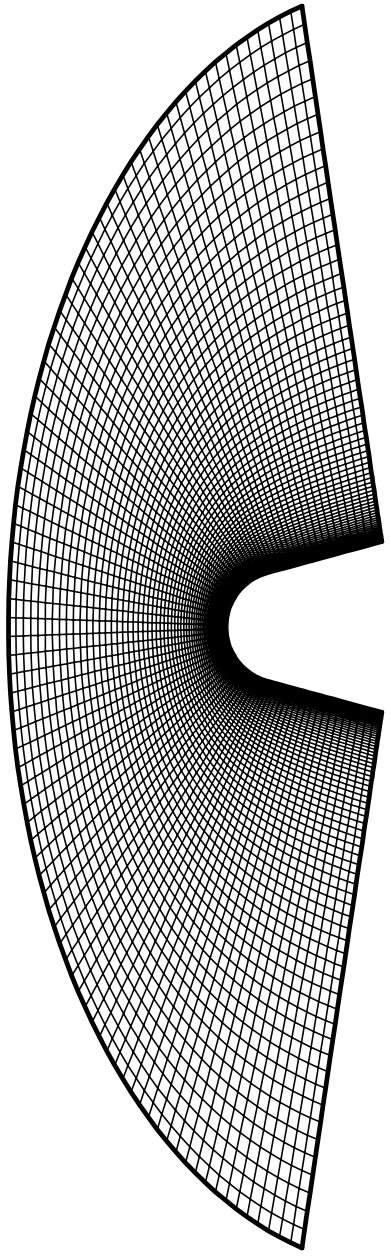

Fig. 7 Computational grid system for blunt-body flow.

2. *Magnetofluid Dynamics Analysis*

To examine the effect of a magnetic field, the decomposed MFD and full MFD equations were used to model hypersonic flow over a blunt body. A uniform field of strength $B_{oy} = 0.02$ T was applied in the y direction, and the applied electric field was set equal to zero. The laminar flow of air with calorically perfect gas assumption was considered for the present analysis. Ionization of the air was assumed to exist in the region between the body and shock wave due to high temperature values in the postshock region. A uniform distribution of electrical conductivity was assumed for the present study. The value of electrical conductivity has been adjusted to achieve a magnetic Reynolds number equal to 1.788, and the interaction parameter is $Q_{\text{ref}} = 0.1$. The magnetic Reynolds number and interaction parameter were computed on the basis of a reference length and free-stream operating conditions.

Because the DMFD equations treat imposed and induced magnetic fields separately, the boundary conditions at the surface for the imposed and induced magnetic field components were specified individually. The induced magnetic field was evaluated at the surface by using Ampere–Maxwell's equation and generalized Ohm's law (details for evaluating the induced magnetic field components were provided in [11]), whereas the imposed magnetic field was prescribed according to the specified distribution.

Figure 10 indicates the pressure contours obtained from MFD analysis by using the DMFD and FMFD formulations. It is interesting to observe that both MFD formulations provide a similar shock structure for the present MFD computations. The effects of the Lorentz force are evident in ionized gas and have resulted in an enlargement of the shock envelope compared with the Navier–Stokes analysis. However, enlargement in the shock structure is high at the body shoulder compared with the stagnation region, which is primarily due to the relatively larger strength of the induced magnetic field away from the stagnation portion. It is important to note that the magnitude of the induced magnetic field increases to substantially larger values than the initially applied field at the region away from the stagnation point and may dominate the fluid stresses. Large values of magnetic field strength result in a strong Lorentz force of $\mathbf{F} = \mathbf{J} \times \mathbf{B}$, where $\mathbf{J}$ is the current density, and $\mathbf{B}$ is the magnetic field vector. The Lorentz force, also known as electromagnetic force, has been generated by the interaction of ionized fluid particles with the magnetic field. Consequently, strong interaction occurs at the body shoulder, thus causing a larger displacement of the shock wave

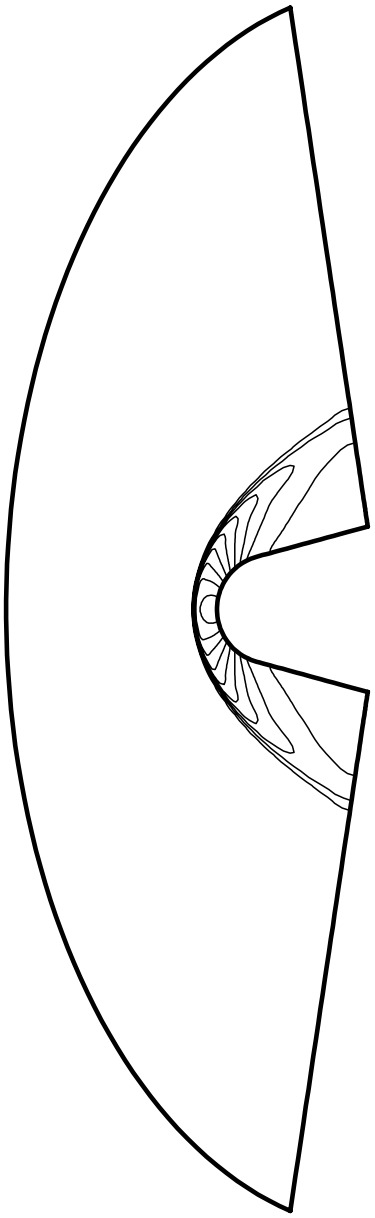

Fig. 8 Pressure contours for the Navier–Stokes computation.

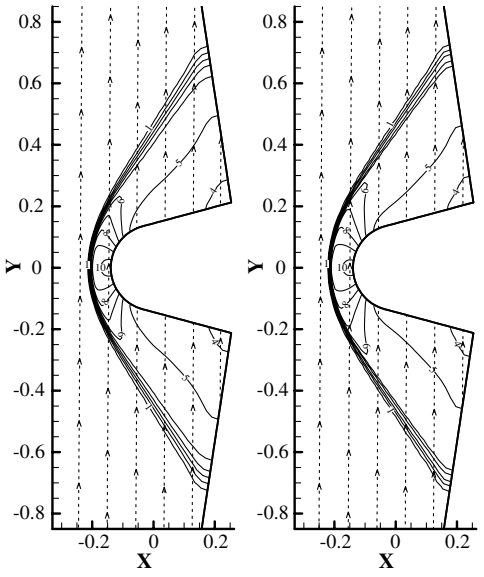

Level	1	2	3	4	5	6	7	8	9	10
P:	500	1000	1500	2000	2500	3000	3500	4000	4500	5000

Fig. 10 Comparison of pressure contours obtained from the DMFD and FMFD formulations with $B_{oy} = 0.02$ T for $R_m = 1.788$.

structure at the shoulder for the applied uniform magnetic field distribution.

Finally, the nondimensional surface pressures along the body surface obtained from the decomposed MFD and full MFD equations are presented in Fig. 11. It is shown that the DMFD formulation predicts a similar change in the pressure distribution as the FMFD formulation for magnetofluid dynamics analysis. A comparison with the Navier–Stokes analysis shows that surface pressure falls off near the stagnation point region after the application of the magnetic field; however, away from the stagnation region, an increase in surface pressure is observed. The increase in surface pressure at the body shoulder indicates a flow-compression phenomenon, which results from strong magnetic interaction. It should be noted that the magnetic interaction parameter is proportional to the square of the magnetic field intensity and reciprocal of the flow velocity. An augmentation of the induced magnetic field strength over a period of time and a significant increase in boundary-layer thickness away from the stagnation portion result in high values of the magnetic interaction parameter; therefore, considerable flow compression has occurred at the shoulder after the application of a magnetic field.

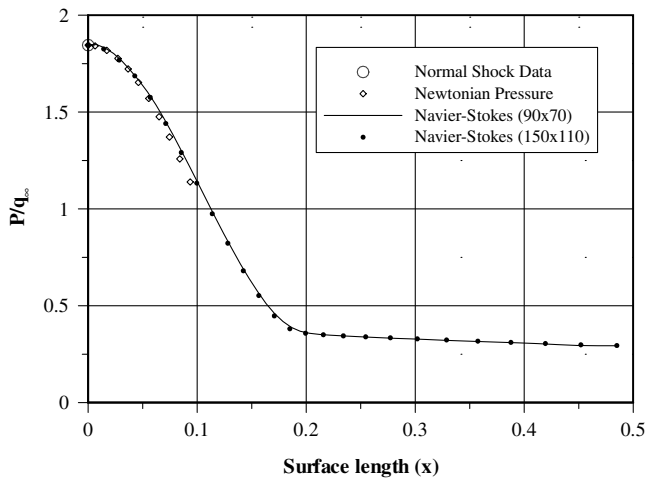

Fig. 9 Surface pressure for the Navier–Stokes analysis.

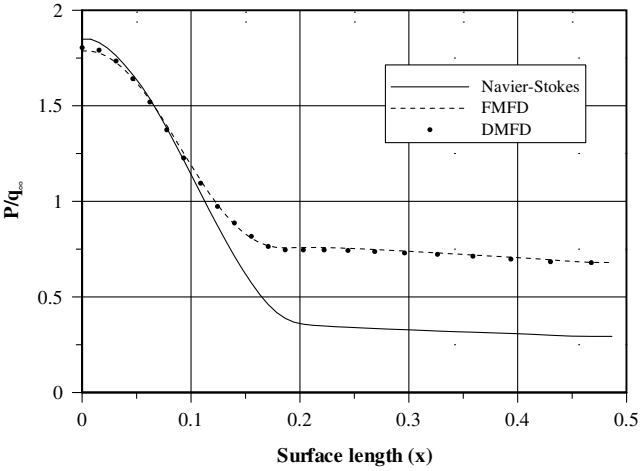

Fig. 11 Comparison of surface pressures obtained from the Navier–Stokes and MFD analyses.

Subsequently, a significantly low value of magnetic Reynolds number equal to $R_m = 2.5 \times 10^{-2}$ has been selected to evaluate the performance of the DMFD formulation. A dipole type of magnetic field distribution has been selected. A strong magnetic field of $B_o = 2.0$ T at the body stagnation point has been generated by placing the dipole at the body center. A significantly large value of the magnetic interaction parameter, $Q_{\text{ref}} = 13.83$, is obtained for this MFD analysis. The pressure contours along with the imposed magnetic field distribution obtained from the DMFD formulation are shown in Fig. 12. An increase in shock standoff distance and an enlargement of the shock envelope are obvious for the present MFD computation. In this case also, the computational time required for the DMFD equations is much smaller than for the FMFD equations for the case with the low range of magnetic Reynolds numbers; however, the difference diminishes as the magnetic Reynolds number increases.

This fact becomes even more clear from Fig. 13, which represents the computational time in terms of wall clock time obtained from the DMFD and FMFD formulations for different ranges of magnetic Reynolds numbers. A dipole was placed at the body center, and a maximum magnetic field strength of 0.6 T was generated at the stagnation point. The computational domain size was increased significantly, primarily due to the FMFD formulation. For the FMFD equations, for which the unknown magnetic field vector consists of induced and imposed components, the accumulation of the magnetic field results in a substantial movement of the shock wave away from the body and the subsequent return of the shock wave toward the body upon dissipation of the accumulated magnetic field. This phenomenon requires a substantially larger domain size when the FMFD equations are used and may result in poor resolution of the shock wave due to an insufficient number of grid points. However, this problem can be avoided when DMFD formulation is used to model the MFD blunt-body flow. In the current analysis, the computational time was evaluated on the same domain size and grid spacing for the two MFD formulations on a dual core microprocessor as described earlier. A close examination of Fig. 13 indicates that the FMFD formulation requires a significantly longer computation time compared with the DMFD formulation for small magnetic Reynolds numbers and a strong imposed magnetic field. For example, at $R_m = 2.5 \times 10^{-2}$, the computational time required by the FMFD equations is approximately 6 times larger than the computational time required by the DMFD equations. It is expected that the FMFD formulation will become more unstable and require a large amount of time as the values of magnetic Reynolds number decrease further. As a result, the difference in computation time will substantially increase. However, with the increase in the values of magnetic Reynolds numbers, the numerical scheme for the FMFD equations becomes stable and requires less time to achieve a converged solution. Finally, for magnetic Reynolds numbers greater than 0.25, both MFD formulations result in the requirement of an almost similar amount of time.

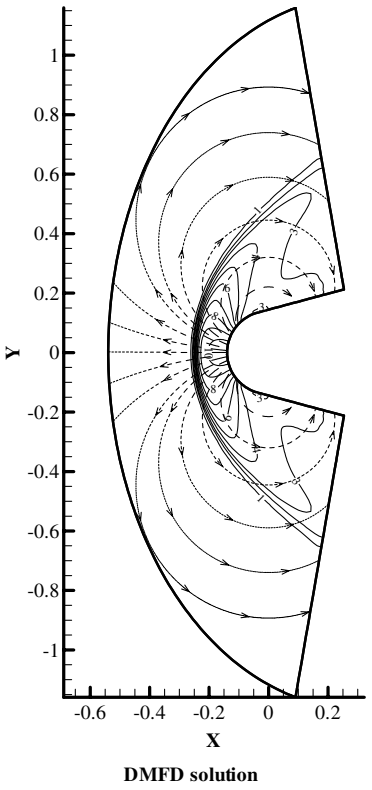

Fig. 12 Pressure contours obtained from the DMFD formulation with $B_o = 2.0$ T for $R_m = 2.5 \times 10^{-2}$.

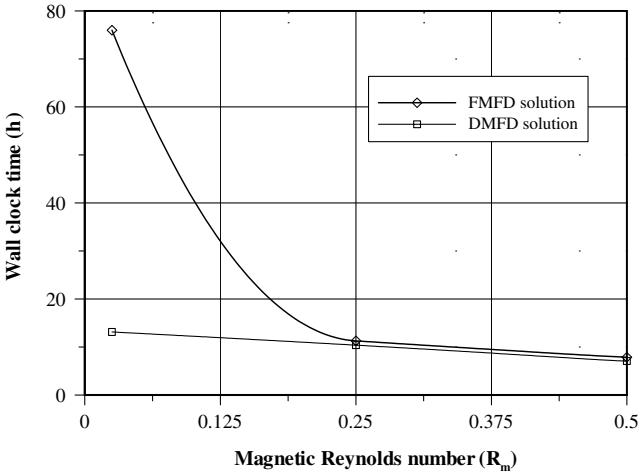

Fig. 13 Comparison of wall clock time for the FMFD and DMFD formulations for hypersonic blunt-body flow computations.

V. Conclusions

An alternate form of full MFD equations, decomposed MFD equations, has been further developed and numerically investigated. An explicit numerical algorithm based on the four-stage modified Runge–Kutta scheme with TVD limiters in the postprocessing stage was successfully used to achieve the numerical solution of the DMFD equations. The developed formulation was validated with two MFD problems: 1) magnetic Rayleigh, and 2) hypersonic blunt-body flow. It has been shown that the alternate form, the DMFD equations, predicts similar results to those of the classical full MFD equations. Based on the magnetic Rayleigh problem, it can be concluded that, for a relatively strong imposed magnetic field, the DMFD equations require substantially less computation time compared with the FMFD equations for low values of magnetic Reynolds number. The low magnetic Reynolds number approach has proven to be the most efficient formulation for achieving the solution and should be used for extremely small values of magnetic Reynolds numbers, such as 0.01 or less. The performance of the DMFD equations exceeds that of the full MFD equations for hypersonic blunt-body flow simulation. At low values of magnetic Reynolds numbers and with a strong imposed magnetic field, the use of the DMFD formulation is recommended, due to the excessive computational requirement of the full MFD formulation.

Acknowledgment

The authors acknowledge the support of Wichita State University's High Performance Computing Center for performing the computational task involved in this research.

References

[1] Gaitonde, D. V., and Poggie, J., "Simulations of Magnetogasdynamics Flow Control Techniques," AIAA Paper 2000-2326, 2000.

[2] Poggie, J., and Gaitonde, D. V., "Computational Studies of Magnetic

Control in Hypersonic Flow," AIAA Paper 2001-0196, 2001.
[3] Hoffmann, K. A., Damevin, H. M., and Dietiker, J. F., "Numerical Simulation of Hypersonic Magnetohydrodynamic Flows," AIAA Paper 2000-2259, 2000.
[4] MacCormack, R. W., "A Conservation Form Method for Magneto-Fluid Dynamics," AIAA Paper 2001-0195, 2001.
[5] MacCormack, R. W., "Flow Calculations with Strong Magnetic Fields," AIAA Paper 2003-3623, 2003.
[6] MacCormack, R. W., "Magneto-Aerodynamic Flow Calculations with Strong Magnetic Fields," AIAA Paper 2004-2163, 2004.
[7] MacCormack, R. W., "Aerodynamic Flow Calculations with Strong Magnetic Induction and Diffusion," AIAA Paper 2005-0559, 2005.
[8] MacCormack, R. W., "Evaluation of the Low Magnetic Reynolds Approximation for Aerodynamic Flow Calculations," AIAA Paper 2005-4780, 2005.
[9] MacCormack, R. W., "Numerical Simulation of Aerodynamic Flow Within a Strong Magnetic Field with Hall Current and Ion Slip," AIAA Paper 2007-4370, 2007.
[10] Khan, O. U., Hoffmann, K. A., and Dietiker, J. F., "Validity of Low Magnetic Reynolds Number Formulation of Magnetofluiddynamics," AIAA Paper 2007-4374, 2007.
[11] Khan, O. U., "Development and Numerical Investigation of Magnetofluiddynamics Formulations," Ph.D. Dissertation, Department of Aerospace Engineering, Wichita State University, Wichita, KS, 2008.
[12] Powell, K. G., Roe, P. L., Myong, R. S., Gombosi, T., and De Zeeuw, D., "An Upwind Scheme for Magnetohydrodynamics," AIAA Paper 1995-1704-C, 1995.
[13] Hoffmann, K. A., and Chiang, S. T., *Computational Fluid Dynamics*, 4th ed., Vol. 2, Engineering Education System, Wichita, Kansas, 2000.
[14] Harada, S., Hoffmann, K. A., and Augustinus, J., "Development of a Modified Runge–Kutta Scheme with TVD Limiters for the Ideal Two-Dimensional MHD Equations," AIAA Paper 98-0981, Jan. 1998.
[15] Moreau, R., *Magnetohydrodynamics*, Kluwer, Dordrecht, The Netherlands, 1990.

D. Gaitonde
Associate Editor